Investigation of Single-Event Burnout Robustness in 1.2 kV SiC Power Devices with Various Edge Termination Structures Under Proton Irradiation

Sangyeob Kim
Department of Electrical and Electronic Engineering
Pusan National University
Busan, Korea
syk@pusan.ac.kr

Jeongtae Kim
Department of Electrical and Electronic Engineering
Pusan National University
Busan, Korea
jtkim99@pusan.ac.kr

Dong-Seok Kim
Korea Atomic Energy Research Institute
Gyeongju, Korea
dongseokkim@kaeri.re.kr

Hyuncheol Bae
Electronics and Telecommunications Research Institute
Daejeon, Korea
hcbae@etri.re.kr

Ogyun Seok
School of Electrical and Electronic Engineering
Pusan National University
Busan, Korea
ogseok@pusan.ac.kr

***Abstract*— Single-event burnout (SEB) in 1.2 kV SiC power devices with various edge termination structures was investigated under proton irradiation. Ring-assisted junction termination extension (RA-JTE), multiple floating zone JTE (MFZ-JTE), and field-limiting rings (FLR) were evaluated using leakage monitoring under reverse-bias conditions. Burnout was predominantly observed when the applied reverse bias exceeded 1.1 kV across the tested structures, except for a single RA-JTE device that exhibited no burnout at 1320 V. Simulation results indicate that SEB susceptibility is governed by where the peak electric field forms during an event with the most vulnerable cases associated with peak electric field formation near the main junction. In RA-JTE, the peak electric field tends to shift toward the main junction side from the irradiation point. These findings emphasize that protecting the main junction is critical for improving edge termination robustness against proton induced SEB.**

Keywords— SiC; Single Event Burnout (SEB); Edge Termination; Proton Irradiation.

I. Introduction

SiC power devices are widely regarded for space and other radiation-prone environments because their wide bandgap and high critical electric field enable reliable high-voltage operation with enhanced radiation hardness compared to conventional silicon devices [1]. In such environments, exposure to high-energy particles, particularly protons, can induce not only gradual degradation mechanisms such as total ionizing dose and displacement damage but also single-event effect that lead to catastrophic failure under reverse-bias operation [2-3].

It is important to note that the trigger for proton-induced single event burnout (SEB) is different from direct heavy-ion strikes. While heavy ions cause SEB directly, protons trigger SEB indirectly by generating high-LET secondary ions through nuclear reactions with the SiC lattice. Therefore, analyzing the impact of these secondary ions is essential to understand the radiation safety of SiC devices. In particular, the design of the edge termination determines the electric field distribution, which significantly affects SEB robustness. However, systematic studies rcomparing SEB characteristics across various termination structures under proton irradiation are still limited.

In this work, we evaluated the proton-induced SEB in 1.2 kV SiC TEGs with RA-JTE, MFZ-JTE, and FLR structures through proton irradiation. By combining GEANT4 to analyze secondary ion effects and TCAD to investigate electric field crowding, we identify the key failure mechanisms and provide design guidance for radiation-hardened SiC power devices.

II. Device Structures and Experiment

Fig. 1 presents the cross-sectional views and layouts of the 1.2 kV SiC TEGs consisting of (a) ring-assisted junction termination extension (RA-JTE), (b) multiple-floating-zone JTE (MFZ-JTE), and (c) field-limiting rings (FLR). The TEGs were fabricated on an N-type drift layer with a thickness of 10 μm and a doping concentration of 8×10^{15} cm^{-3}. To evaluate the termination behavior under proton-induced SEB conditions, active regions were intentionally excluded from the TEG design. The detailed design methodology and parameter selection procedures are described in [4]. Following the fabrication process, A 6-inch wafer was diced into individual chips and subsequently encapsulated in standard TO-247 packages. Wire bonding was performed to establish electrical connections, enabling the application of high-voltage reverse bias and in-situ monitoring of the leakage current during proton irradiation. Fig. 2 illustrates (top-left) the top-view layout of the diced chip, (top-right) the die-attached lead frame, and

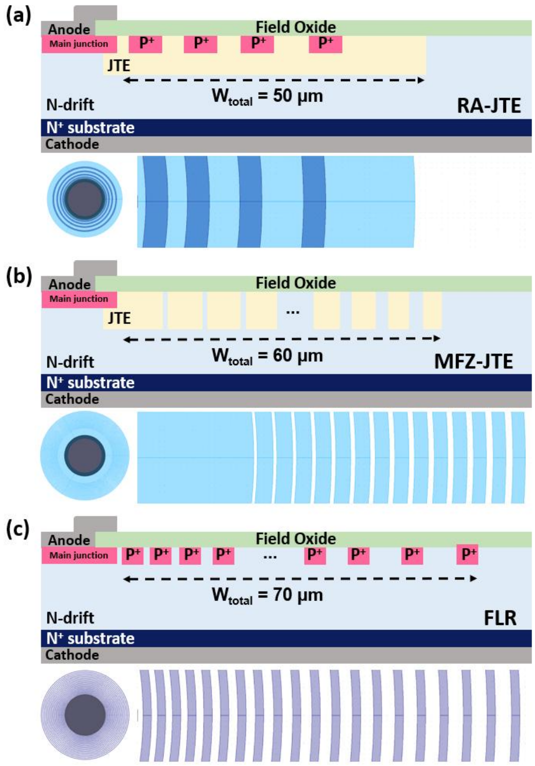

Fig. 1. Cross-sectional views and layouts of the 1.2 kV SiC edge-termination TEGs employing (a) RA-JTE, (b) MFZ-JTE, and (c) FLR.

and (bottom) the final packaged samples prepared for the SEB experiments.

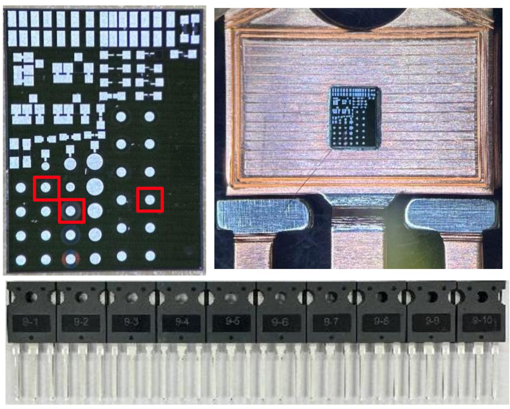

Fig. 2. (top-left) the top-view layout of the diced chip, (top-right) the die-attached lead frame, and (bottom) the final packaged samples.

Proton irradiation were performed at the Korea Multi-purpose Accelerator Complex (KOMAC) of the Korea Atomic Energy Research Institute (KAERI) with an incident energy of 100 MeV. During the irradiation process, various voltage ratio [biased reverse voltage (V_R) / breakdown voltage (BV)] conditions were applied to the devices, as summarized in Table I. The leakage current was monitored in situ to detect the occurrence of SEB and to capture the real-time breakdown behavior of each edge termination structure.

TABLE I. CONDITIONS OF BIAS VOLTAGE DURING IRRADIATION

Sample ID	BV [V]	V_R [V]	Voltage ratio [%]
RA-1	1640	984	60
RA-2	1637	1146	70
RA-3	1648	1319	80
RA-4	1651	1320	80
RA-5	1627	1464	90
MFZ-1	1629	978	60
MFZ-2	1606	1124	70
MFZ-3	1609	1287	80
MFZ-4	1626	1300	80
FLR-1	1276	893	70
FLR-2	1365	1092	80
FLR-3	931	744	80
FLR-4	1452	1307	90

A precision high-voltage power supply was employed to apply the reverse bias, while a picoammeter was used for real-time in-situ leakage current monitoring. The anode and cathode electrode of the packaged sample were connected to the measurement equipment to enable simultaneous bias application and current measurement during high bias and high energy proton irradiation. The proton flux was regulated at approximately 1.3×10^{11} cm^{-2}·s^{-1}. For each test, irradiation was immediately terminated upon the detection of an SEB event; otherwise, the exposure was continued until reaching a predefined total fluence of 1×10^{13} cm^{-2}.

III. RESULTS AND DISCCUSIONS

Fig. 3 illustrates the transient leakage current responses for the (a) RA-JTE, (b) MFZ-JTE, and (c) FLR structures during proton irradiation with energy of 100 MeV. The irradiation interval is marked by the "Start" and "Stop" points, and each trace was monitored continuously while a constant reverse bias was applied. To protect the measurement system, a current compliance of 100 mA was set; any device exceeding this limit was identified as a burnout failure, leading to immediate test termination.

For the RA-JTE and MFZ-JTE designs, burnout was generally observed at biases ≥70% of their respective breakdown voltages (BVs). Notably, no burnout was observed in RA-4 sample representing a unique exception. In the FLR case, although a non-burnout event was recorded for FLR-3, this sample had a lower pre-irradiation BV compared to the

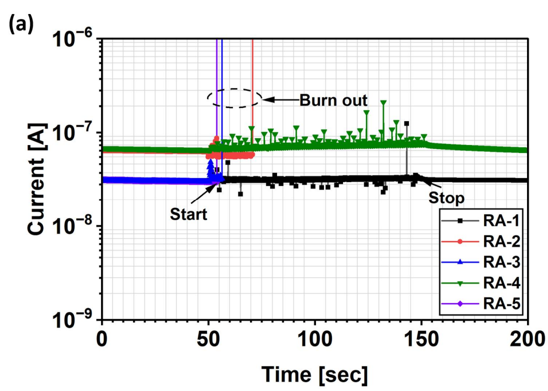

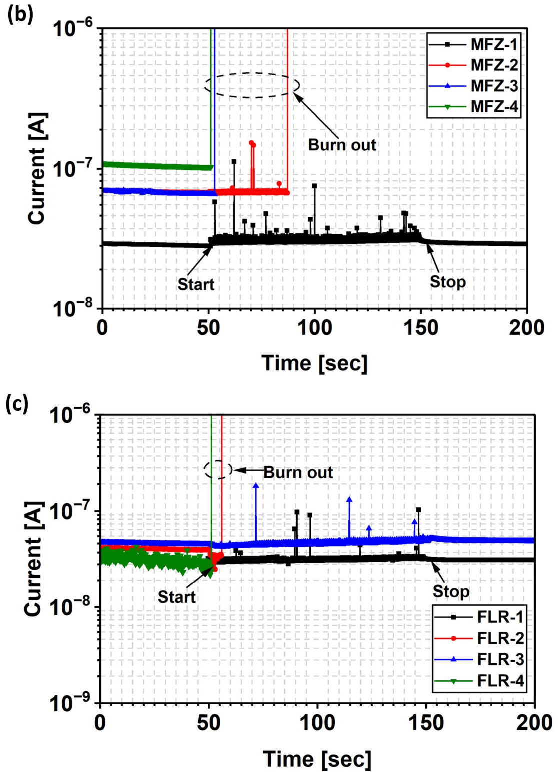

Fig. 3. Transient leakage current responses for the (a) RA-JTE, (b) MFZ-JTE, and (c) FLR structures during proton irradiation with energy of 100 MeV.

others. This implies that the actual absolute voltage stress was lower, which likely prevented the onset of SEB.

Fig. 4 summarizes the SEB results by mapping the reverse bias conditions against the proton fluence. Although the stress conditions followed voltage ratios, the failures exhibit a stronger correlation with the absolute reverse bias level than the termination type. Specifically, burnout events were predominantly observed above a threshold of ~1.1 kV, whereas devices biased below this level remained stable up to the maximum fluence. Excluding one RA-JTE sample at 1320 V, SEB occurrence is more accurately governed by the absolute reverse bias level than the relative voltage ratio.

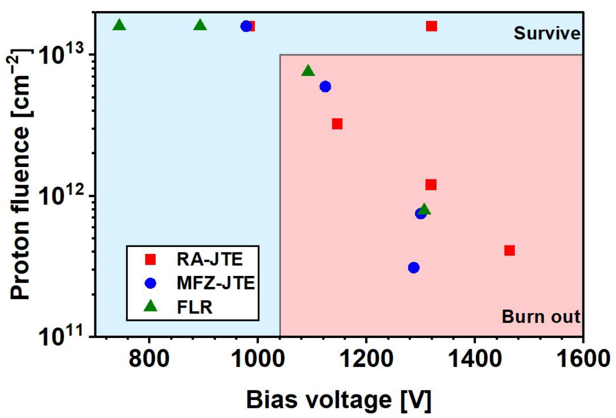

Fig. 4. SEB results by mapping the reverse bias conditions against the proton fluence for SiC edge termination TEGs.

To establish the LET input for TCAD simulations, the LET spectrum in SiC under proton irradiation with energy of 100 MeV was extracted via GEANT4, accounting for secondary particles (Fig. 5). Based on this distribution, a representative LET of 16 MeV·cm²/mg was selected, corresponding to a charge-line density of 0.1 pC/μm. The ion track was configured for normal incidence to the surface, with additional track parameters summarized including LET, lateral straggle length (L_{st}), penetration depth (D_p), initial irradiation time, tilt angle, and V_R in Table II.

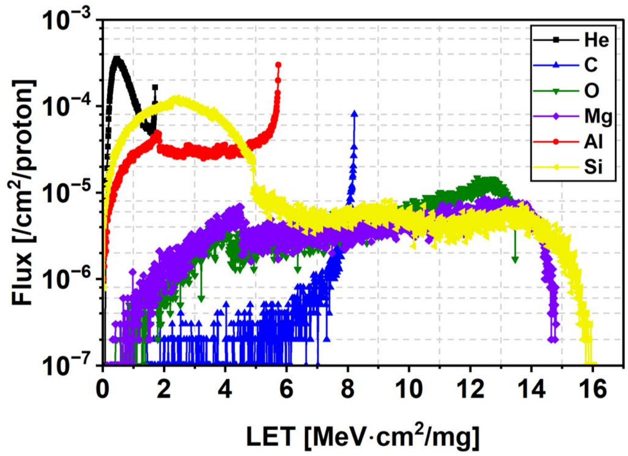

Fig. 5. LET distributions of secondary particles in SiC induced by proton irradiation with energy of 100 MeV extracted thurough GEANT4.

Fig. 6 presents the transient vertical and horizontal electric field distributions for the (a, b) RA-JTE, (c, d) MFZ-JTE, and (e, f) FLR structures following a particle strike at the main junction (V_R = 1200 V). In all designs, the peak electric field occurs at transient time of 20 ps, with significant electric field enhancement commonly observed at both the drift/substrate interface and the main junction region. Notably, the RA-JTE exhibits reduced electric field crowding at the main junction due to the P^+ ring assisted field redistribution, keeping the peak junction field below 3 MV/cm, whereas MFZ-JTE and FLR show a sharper transient field concentration that exceeds 3 MV/cm. This reduced peak in RA-JTE accounts for the exceptional non-burnout at 1320 V, whereas other structures failed predominantly once the bias exceeded the 1.1 kV threshold.

Fig. 7 presents the simulated lattice temperature profiles for the three termination structures following a particle strike. The temperature evolution follows a similar trend across all designs, with minimal difference between structures. The FLR structure exhibits the highest peak lattice temperature of 576.8 K, while the RA-JTE and MFZ-JTE maintain lower values. Crucially, these peaks remain well below the Al melting point (895.4 K), suggesting that thermal overheating is not the primary trigger for SEB under these conditions. Instead, the findings suggest that SEB is governed by electric field-induced impact ionization rather than thermal overheating.

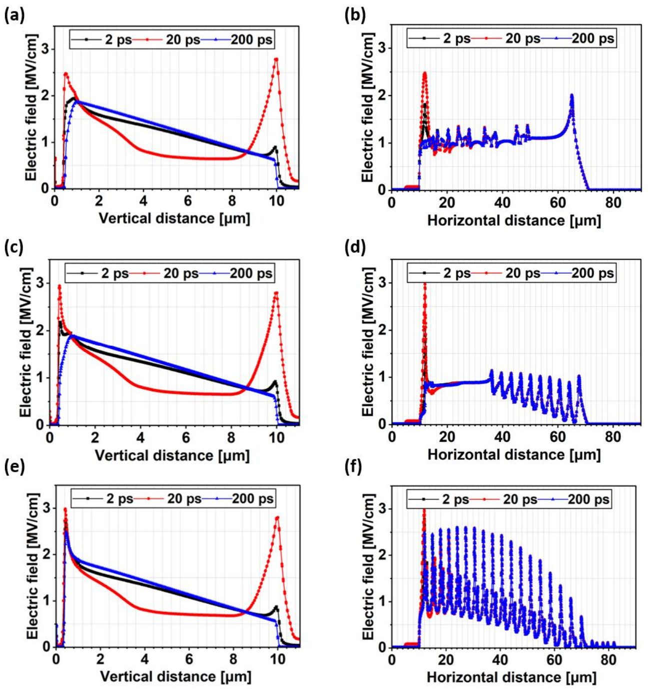

Fig. 6. Vertical and horizontal electric field distributions of the (a), (b) RA-JTE, (c), (d) MFZ-JTE, and (e), (f) FLR structures at different time points after a particle strike applied to the main junction under a drain bias of 1200 V.

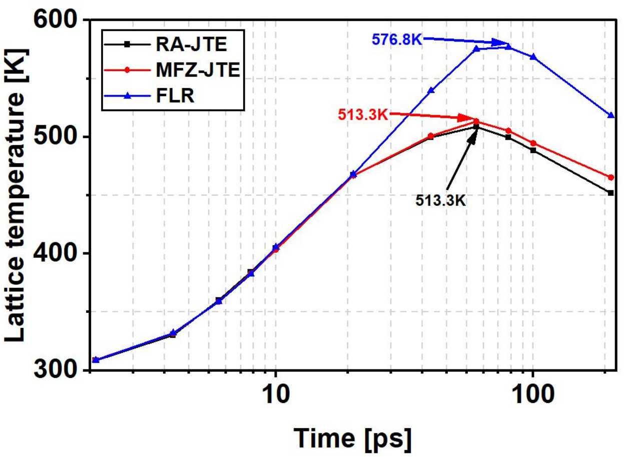

Fig. 7. Lattice temperature after a particle strike for the RA-JTE, MFZ-JTE, and FLR under a drain bias of 1200 V.

Fig. 8 illustrates the electric field distributions in the RA-JTE structure for various lateral strike locations, as indicated by red arrows. Three representative positions are considered: the main junction, the edge of the last P^+ ring, and the end of the JTE region. In all cases, the maximum electric field does not remain at the strike point but tends to develop toward the main junction side. This consistent hotspot migration indicates that the main junction adjacent region governs the critical electric field condition during an event. Therefore, JTE designs for SEB robustness should be focused on effectively protecting the main junction.

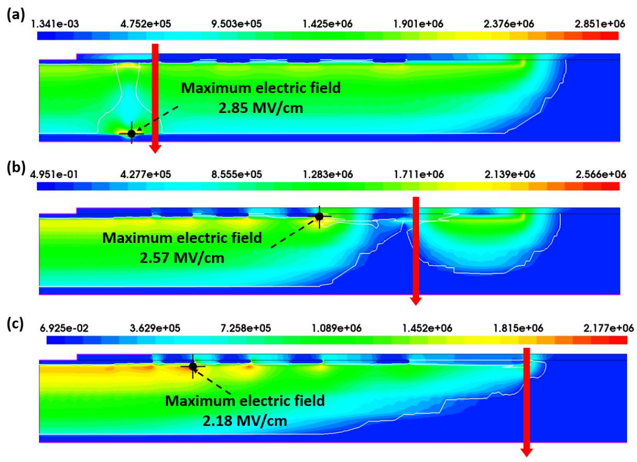

Fig. 8. Electric field distributions in the RA-JTE structure for various lateral strike locations of (a) main junction, (b) last P^+ ring, and (c) end of the JTE region under a drain bias of 1200 V.

IV. Conclusion

This work investigated proton-induced SEB in 1.2 kV SiC edge termination TEGs featuring RA-JTE, MFZ-JTE, and FLR under proton irradiation with energy of 100 MeV. While stress conditions were initially based on voltage ratios, SEB failures exhibited a stronger dependence on the absolute bias level than the termination type, occurring predominantly above a 1.1 kV threshold. TCAD simulations revealed that SEB is triggered by transient electric field crowding near the main junction rather than thermal overheating. The RA-JTE demonstrated superior robustness by effectively suppressing this electric field enhancement (< 3 MV/cm) through multiple P^+ ring-assisted redistribution. These results emphasize that enhancing SEB robustness in high-voltage SiC devices requires optimized electric field mitigation specifically in regions adjacent to the main junction.

Acknowledgment

This research was supported by the National Research Council of Science & Technology(NST) grant by the Korea government (MSIT) (Aerospace Semiconductor Strategy Research Project No. GTL25052-104) and the MSIT(Ministry of Science and ICT), Korea, under the ITRC(Information Technology Research Center) support program(IITP-2025-RS-2024-00438288) supervised by the IITP(Institute for Information & Communications Technology Planning & Evaluation) and National Research Foundation (NRF) funded by the Korean government (MSIT) (RS-2024-00437064).

References

[1] L. Spaziani and L. Lu, ''Silicon, GaN and SiC: There's room for all: An application space overview of device considerations,'' in Proc. IEEE 30th Int. Symp. Power Semiconductor Devices & ICs (ISPSD), May 2018, pp. 8–11.

[2] C. Kim, H. Yoon, D.-S. Kim, and O. Seok, "Comparison analysis of radiation effects on 1.2 kV SiC metal-oxide-semiconductor fieldeffect transistors with gamma-ray and proton irradiation," Electronics vol. 13, no. 7, 1352, Apr. 2024.

[3] C. Peng et al., "Mono-energetic proton induced damages in SiC power MOSFETs," IEEE Trans. Device Mater. Rel., vol. 23, no. 1, pp. 64–71, Mar. 2023.

[4] S. Kim, J. Kim, D.-S. Kim, H. Bae, G. Kang, and O. Seok, ''Effects of Proton Irradiation on SiC Power Devices with Various Edge Termination Structures,'' in Proc. IEEE 37th Int. Symp. Power Semiconductor Devices & ICs (ISPSD), June 2025, pp. 565–568.